Available online at www.sciencedirect.com
SCIENCE DIRECT®
International Journal of Heat and Mass Transfer 48 (2005) 1952–1960
International Journal of HEAT and MASS TRANSFER
www.elsevier.com/locate/ijhmt

Three-dimensional thermocapillary-buoyancy flow in a shallow molten silicon pool with Cz configuration

You-Rong Li [a,*], Xiao-Jun Quan [a], Lan Peng [a], Nobuyuki Imaishi [b], Shuang-Ying Wu [a], Dan-Ling Zeng [a]

[a] College of Power Engineering, Chongqing University, Chongqing 400044, China
[b] Institute for Materials Chemistry and Engineering, Kyushu University, Fukuoka, Japan

Received 2 March 2004; received in revised form 30 November 2004
Available online 19 February 2005

Abstract

In order to understand the characteristics of surface patterns on silicon melt in Czochralski furnaces, we conducted a series of unsteady three-dimensional numerical simulations of thermocapillary-buoyancy flow of a shallow molten silicon pool with Czochralski configuration (depth $d = 3$ mm). The crucible sidewall is maintained at constant temperature. Bottom and free surfaces are adiabatic or allow heat transfer in the vertical direction. The simulation results indicate that two flow transitions occur with increasing the radial temperature difference along the free surface. At first, the steady two-dimensional flow becomes steady three-dimensional flow and then oscillatory three-dimensional flow. The critical conditions for the onset of the instability were determined. Characteristics of the steady and the oscillatory three-dimensional flows were discussed.

Keywords: Computer simulation; Thermocapillary-buoyancy flow; Spoke pattern; Czochralski method; Silicon melt

1. Introduction

The Czochralski (Cz) method is one of the most important methods of producing silicon single crystal from the melt. In this method, the buoyancy and thermocapillary forces are coupled to cause the melt convection. Smith and Davis [1] performed the linear stability analysis of thermocapillary flow in a thin and infinitely extended fluid layer with a free upper surface subjected to a constant horizontal temperature gradient. They found two types of three-dimensional (3-D) instabilities, i.e. stationary longitudinal rolls and oblique hydrothermal waves depending on the Prandtl number (Pr) and the basic flow pattern (with or without a return flow), and determined the critical Marangoni number (Ma). Subsequently, the extension of Smith and Davis' theory to account for the influence of buoyancy forces was done by Laure and Roux [2] for the low-Pr fluids. At the same time, Yamagishi and Fusegawa [3] performed the experiment of thermocapillary-buoyancy flow and observed dark lines at the surface of the melt by CCD camera during silicon Cz growth. Since this pattern looks like the spoke of a wheel, it is called a spoke pattern. Furthermore, Yi et al. [4] performed a 3-D numerical simulation of the silicon melt flow and verified asymmetric temperature profiles similar to the spoke patterns and related

* Corresponding author. Tel.: +86 23 6511 2284; fax: +86 23 6510 2473.
E-mail address: liyourong@yahoo.com (Y.-R. Li).

0017-9310/$ - see front matter © 2005 Elsevier Ltd. All rights reserved.
doi:10.1016/j.ijheatmasstransfer.2004.11.024

Nomenclature

A_m	amplitude of temperature oscillation, K
Bo	Bond number, Eq. (11)
C_p	heat capacity, J kg^{-1} K^{-1}
d	depth, m
$\boldsymbol{e}_z$	z-directional unit vector
g	gravitational acceleration, m s^{-2}
m	azimuthal wave number
Ma	Marangoni number, Eq. (9)
p	pressure, Pa
Pr	Prandtl number, $Pr = \nu/\alpha$
q	heat flux, W m^{-2}
r	radius, m
Ra	Rayleigh number, Eq. (10)
t	time, s
T	temperature, K
$\boldsymbol{V}$	velocity vector
z	axial coordinate, m

Greek symbols

α	thermal diffusivity, m^2 s^{-1}
β	growth rate constant, s^{-1}
γ_T	temperature coefficient of surface tension, N m^{-1} K^{-1}
ε	emissivity of the melt
θ	azimuthal coordinate, rad
λ	thermal conductivity, W m^{-1} K^{-1}
μ	dynamic viscosity, kg · m^{-1} s^{-1}
ν	kinematic viscosity, m^2 s^{-1}
ρ	density of the melt, kg m^{-3}
ρ_T	thermal expansion coefficient of the melt, K^{-1}
σ	Stefan–Boltzmann constant, W m^{-2} K^{-4}
ψ	stream function, m^3 s^{-1}
ω	angular velocity of hydrothermal waves, rad s^{-1}

Subscripts

a	ambient
c	crucible
cri	critical
H	heated
m	melting point
r	radial
s	crystal
z	axial
θ	azimuthal

asymmetric flow in the silicon melt. They concluded that the Rayleigh–Benard or Marangoni–Benard instability (or both) can cause spoke patterns in the silicon melt. Nakamura [5] observed the thermal waves due to a non-axisymmetric flow at a Czochralski-type silicon-melt surface with a carbon-dummy crystal when the crucible rotates. It is found that the thermal wave number increased with increasing of the crucible rotation rate and the traveling rate of the thermal wave in the azimuthal direction was slower than the crucible rotation rate. Recently, Azami et al. [6] observed the moving spoke patterns on the free surface of a shallow pool of high-temperature silicon melt (3 mm and 8 mm in depth) and reported that thermocapillary flow may play an important role in the incipience of the 3-D convection and the number of spokes. In our previous paper [7], we conducted series of unsteady 3-D numerical simulations of thermocapillary and thermocapillary-buoyancy flows of silicon melt in a shallow annular pool heated from the outer wall and cooled at the inner cylindrical wall and verified the existence of the hydrothermal waves. In the present study, we report a series of numerical simulation on the thermocapillary-buoyancy flow in a shallow pool of silicon melt which is heated from the outer wall and cooled at the cylindrical inner rod which touches the surface of the melt just like the Cz configuration and is the same geometry as that of the experimental apparatus of Azami et al. [6].

2. Model formulation and methodology

We analyze the thermocapillary-buoyancy flow of silicon melt in a shallow molten silicon pool with Cz configuration, as shown schematically in Fig. 1. Radius of the cylindrical rod (hereafter we call this "crystal") is $r_s = 15$ mm, the crucible radius $r_c = 50$ mm and the depth is $d = 3$ mm. The melt/crystal interface and crucible sidewall are maintained at constant temperatures T_s and $T_H > T_s = T_m$, respectively. T_m (=1683 K) is the melting point temperature of silicon. The following assumptions are introduced in our model:

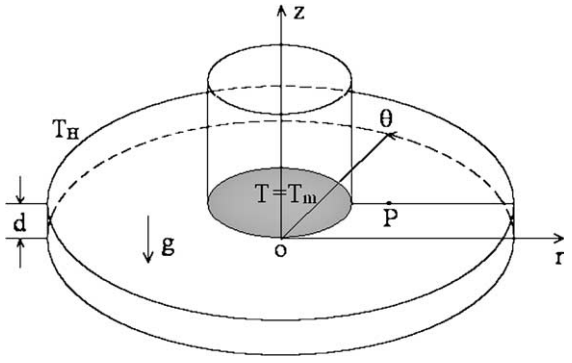

Fig. 1. Configuration of the system.

(1) Silicon melt is an incompressible Newtonian fluid satisfying the Boussinessq approximation except for the surface tension. (2) The velocity is small and the flow is laminar. (3) The upper surface is flat and non-deformable.

At the free surface, the thermocapillary force is taken into account. On every solid–liquid boundary, the no-slip condition is applied. In order to evaluate the effect of vertical heat flux, we introduced two types of thermal boundary conditions on the free and bottom surfaces, i.e., case A: adiabatic on the free and bottom surfaces, and case B: heated at the bottom surface with a constant heat flux ($q = 3\ \mathrm{W\ cm^{-2}}$) and radiative heat loss to the ambient at an effective temperature $T_a = 1599$ K from the free surface. The thermophysical properties of silicon melt at $T_m = 1683$ K is listed in Table 1.

With the above assumptions, the flow and heat transfer equations are expressed as follows:

$$\nabla \cdot \boldsymbol{V} = 0, \tag{1}$$

$$\frac{\partial \boldsymbol{V}}{\partial t} + \boldsymbol{V} \cdot \nabla \boldsymbol{V} = -\frac{1}{\rho}\nabla P + \nu \nabla^2 \boldsymbol{V} + \rho_T g (T - T_m)\boldsymbol{e}_z, \tag{2}$$

$$\frac{\partial T}{\partial t} + \boldsymbol{V} \cdot \nabla T = \alpha \nabla^2 T. \tag{3}$$

The initial conditions are expressed as follows (at $t = 0$):

$$V_r = 0, \tag{4a}$$

$$V_\theta = 0, \tag{4b}$$

$$V_z = 0, \tag{4c}$$

$$T = T_m, \quad r \leqslant r_s \tag{4d}$$

$$T = T_H - (T_H - T_m)\frac{\ln(r/r_c)}{\ln(r_s/r_c)}, \quad r > r_s \tag{4e}$$

The boundary conditions at the free surface ($z = d$, $r_s < r < r_c$, $0 \leqslant \theta < 2\pi$)

$$\mu \frac{\partial V_r}{\partial z} = \gamma_T \frac{\partial T}{\partial r} \tag{5a}$$

$$\mu \frac{\partial V_\theta}{\partial z} = \gamma_T \frac{\partial T}{r\partial \theta}, \tag{5b}$$

$$V_z = 0, \tag{5c}$$

$$\frac{\partial T}{\partial z} = 0 \quad \text{or} \quad -\lambda \frac{\partial T}{\partial z} = \varepsilon\sigma(T^4 - T_a^4), \tag{5d}$$

at the melt/crystal interface ($r \leqslant r_s$, $0 \leqslant z \leqslant d$, $0 \leqslant \theta < 2\pi$)

$$V_r = 0, \tag{6a}$$

$$V_\theta = 0, \tag{6b}$$

$$V_z = 0, \tag{6c}$$

$$T = T_m, \tag{6d}$$

at the bottom ($z = 0$, $r < r_c$, $0 \leqslant \theta < 2\pi$)

$$V_r = 0, \tag{7a}$$

$$V_\theta = 0, \tag{7b}$$

$$V_z = 0, \tag{7c}$$

$$\frac{\partial T}{\partial z} = 0 \quad \text{or} \quad -\lambda \frac{\partial T}{\partial z} = q \tag{7d}$$

at the crucible sidewall ($r = r_c$, $0 \leqslant z \leqslant d$, $0 \leqslant \theta < 2\pi$)

$$V_r = 0, \tag{8a}$$

$$V_\theta = 0, \tag{8b}$$

$$V_z = 0, \tag{8c}$$

$$T = T_H. \tag{8d}$$

The overall temperature difference ($\Delta T = T_H - T_m$) in the radial direction and the effect of the gravity are expressed by the Marangoni number and the Rayleigh number, respectively:

$$Ma = \frac{\gamma_T(\partial T/\partial r)d^2}{\mu\alpha} \approx \frac{\gamma_T d^2}{\mu\alpha}\frac{\Delta T}{r_c - r_s}, \tag{9}$$

$$Ra = \frac{g\rho_T(\partial T/\partial r)d^4}{\nu\alpha}. \tag{10}$$

The relative strength of the buoyancy convection compared to thermocapillary flow can be qualified in terms of the dynamic Bond number

$$Bo = Ra/Ma = \frac{\rho g \rho_T d^2}{\gamma_T} \tag{11}$$

The fundamental equations are discretized by the finite difference method. The modified central difference approximation is applied to the diffusion terms while the QUICK scheme is used for the convective terms. The SIMPLE algorithm [8] is used to handle the pressure-velocity coupling. In this study, nonuniform

Table 1
Physical properties

Symbol	Value	Unit
T_m	1683	K
λ	64	$\mathrm{W\ m^{-1}\ K^{-1}}$
ρ	2530	$\mathrm{kg\ m^{-3}}$
μ	7.0×10^{-4}	$\mathrm{kg\ m^{-1}\ s^{-1}}$
C_p	1000	$\mathrm{J\ kg^{-1}\ K^{-1}}$
ρ_T	1.5×10^{-4}	$\mathrm{K^{-1}}$
γ_T	-7.0×10^{-5}	$\mathrm{N\ m^{-1}\ K^{-1}}$
Pr	0.011	–
ε	0.318	–

staggered grids of $62^r \times 22^z \times 60^\theta$ are used. The validation of the code for the thermocapillary and thermocapillary-buoyancy flow simulation was checked in our previous works [7,9].

Numerical simulations were conducted on an MPU of the Fujitsu VPP700 at the Computer Center of Kyushu University. The time increment was chosen between 0.9 and 2.7×10^{-3} s. The convergence at each time step was assumed if the maximum residual error of the continuity equation among all control volumes became less than $10^{-5}\ s^{-1}$.

3. Results and discussion

3.1. Basic flow

When the radial temperature gradient is small, the thermocapillary-buoyancy flow is steady and axisymmetric. This type of flow is called as the "basic flow". The velocity field is displayed in terms of the stream function ψ, which is defined as

$$V_r = \frac{1}{r}\frac{\partial \psi}{\partial z}, \tag{12a}$$

$$V_z = -\frac{1}{r}\frac{\partial \psi}{\partial r}. \tag{12b}$$

This definition results in positive value of ψ for a counter-clockwise flow and negative for clockwise flow.

When $\Delta T(Ma)$ is very small, the basic thermocapillary-bouyancy flow of silicon melt appears as an axisymmetric steady radial flow with a single convection roll cell. The free surface fluid flows from the outer wall to the crystal. A return flow is dominant near the bottom. The strength of the basic flow increases as $\Delta T(Ma)$ increases. A second co-rotating roll cell appears below the free surface when $\Delta T(Ma)$ is increased, as shown in Fig. 2(a) and (b) for cases A and B, respectively. The maximum stream function of the basic flow localizes near the periphery of the crystal. Obviously, the flow structure is quite insensitive to the thermal boundary conditions on the free and bottom surface. It should be noted that the melt below the crystal is almost stagnant.

For case A, the temperature distribution in the radial direction is almost independent of the presence of the melt flow, since the thermal conductivity of the silicon melt is large. For case B, the radial temperature distributions are strongly dependent on the heat fluxes at the top and bottom surfaces, as shown in Fig. 2(a). Fig. 2(d) shows the distribution of the radial surface velocity (V_r) as a function of radial coordinate. Because large radial temperature drops appear near the crystal, the surface velocity exhibits a sharp peak near the crystal.

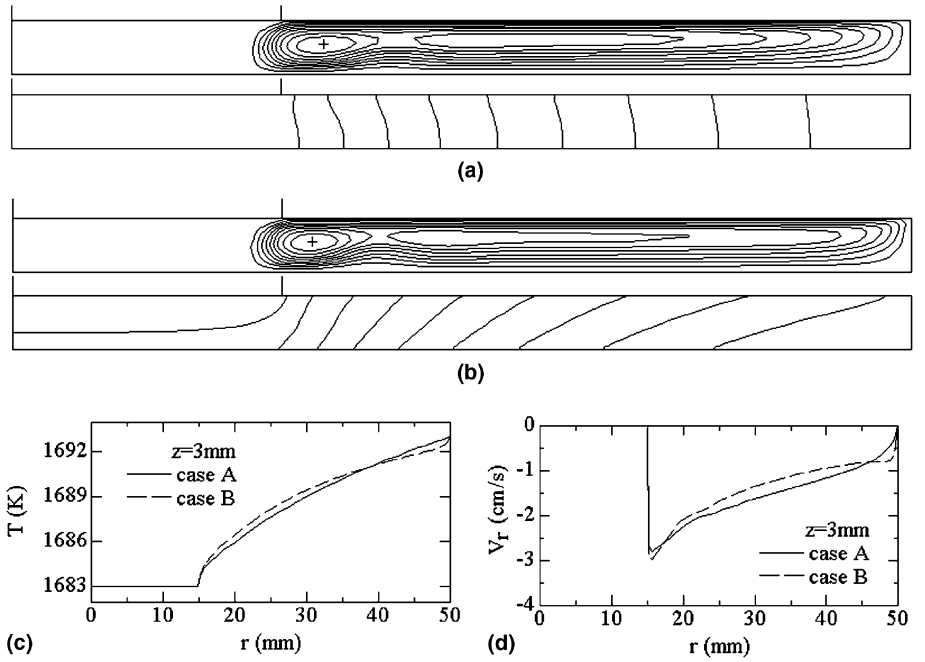

Fig. 2. Characteristics of the basic flow under sub-critical ΔT: (a) streamlines and isotherms for case A at $\Delta T = 10$ K ($Ma = 10.2$), $\psi(+) = 0.25\ cm^3\ s^{-1}$, $\psi(-) = -0.01\ cm^3\ s^{-1}$, $\delta\psi(\psi(+) - \psi(-))/10$, $\delta T = 1$ K; (b) streamlines and isotherms for case B at $\Delta T = 10$ K($Ma = 10.2$), $\psi(+) = 0.26\ cm^3\ s^{-1}$, $\psi(-) = -0.01\ cm^3\ s^{-1}$, $\delta\psi(\psi(+) - \psi(-))/10$, $\delta T = 1$ K; (c) distributions of the surface temperature as a function of radius r; (d) distributions of radial surface velocity (V_r) as a function of radius r.

3.2. Steady three-dimensional flow

When $\Delta T(Ma)$ exceeds a certain threshold value, 3-D disturbances start an exponential growth and finally a steady 3-D flow field is established. The mode and growth process of the 3-D disturbance are characterized by the azimuthal wave number m and the growth rate constant β. The growth of any 3-D disturbance (X) can be expressed by Eq. (13)

$$X(r,\theta,z,t) = X_0(r,\theta,z,0)\sin(2\pi m\theta)\exp(\beta t). \quad (13)$$

In order to extract the 3-D disturbances, we define the fluctuation δX of a physical quantity X as follows:

$$\delta X(r,\theta,d,t) = X(r,\theta,d,t) - \frac{1}{2\pi}\int_0^{2\pi} X(r,\theta,d,t)\mathrm{d}\theta \quad (14)$$

Typical examples of growth of the azimuthal velocity at the monitoring point $P(r = 20$ mm, $\theta = 0)$ are shown in Fig. 3(a). A slope of the semi-logarithmic plot of V_θ vs. t provides the β value. From a plot of β vs. $\Delta T(Ma)$, as shown in Fig. 3(b), we can determine the first critical temperature differences ΔT_{cri1} which corresponds to a state of the neutral stability limit ($\beta = 0$). The first critical temperature differences ΔT_{cri1} and the corresponding critical Marangoni numbers Ma_{cri1} are listed in Table 2, together with the results of the previous work [7].

Once the 3-D disturbance starts, spoke patterns appear on the melt free surface. In this case, the spoke patterns are stationary, as shown in Fig. 4(a) and (b). These stationary spoke patterns correspond to a series of circulating flow cells as shown in Fig. 5 lined up side by side in the azimuthal direction. Structure of these secondary flow cells can be understood from the distributions of the fluctuation velocity and temperature on two r–z planes (O–A and O–B in Fig. 5(a) and (b), respectively) and two $\theta - z$ planes, shown in Fig. 5(c–d). With increasing $\Delta T(Ma)$, the number of spoke patterns decreases and the amplitude of temperature oscillations at the monitoring point P increases slightly, as shown in Fig. 6. However, in a thin annular pool of silicon melt, the steady 3-D flow does not appear and the steady 2-D flow exhibits direct transition to an oscillatory 3-D flow because of the effect of the inner cylinder.

3.3. Oscillatory three-dimensional flow

When $\Delta T(Ma)$ exceeds a second threshold value, the 3-D stationary flow field becomes unstable and the whole flow field starts rotating motion in azimuthal direction with a constant angular velocity, ω. The oscillation amplitudes increase exponentially with time. Present numerical simulations with large ΔT show that during the initial growth process the intensity of any disturbance (X) can be expressed by Eq. (15),

$$X(r,\theta,z,t) = X_0(r,\theta,z,0)\exp[(\beta + \mathrm{i}\beta_I)t)]. \quad (15)$$

Fig. 7(a) shows the growth process of the azimuthal velocity at monitoring point P for the case A at $\Delta T = 18$ K ($Ma = 18.3$). The second critical temperature difference ΔT_{cri2} determined from a plot of β vs. $\Delta T(Ma)$

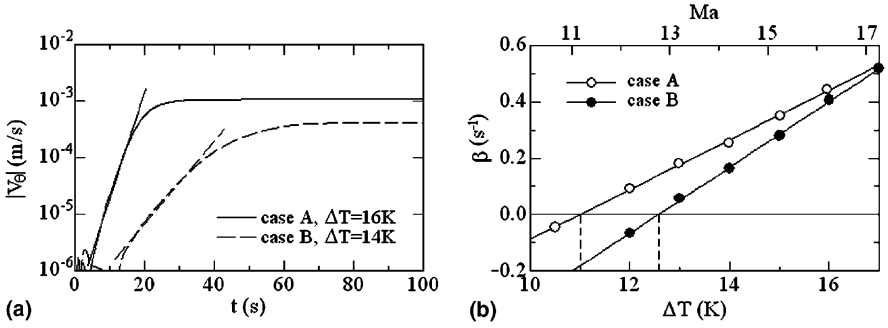

Fig. 3. Determination of the first critical point: (a) growth of the azimuthal velocity disturbances at monitoring point P and (b) β vs. $\Delta T(Ma)$ plot for determining $\Delta T_{cri1}(Ma_{cri1})$.

Table 2
The critical temperature difference ΔT_{cri} and Marangoni number Ma_{cri}

Configuration	Transition point	Case A		Case B	
		ΔT_{cri}	Ma_{cri}	ΔT_{cri}	Ma_{cri}
Pool with the Cz configuration	First critical point	11.0	11.2	12.6	12.8
	Second critical point	17.4	17.7	18.2	18.5
Annular pool [7]		9.0	9.1	7.3	7.5

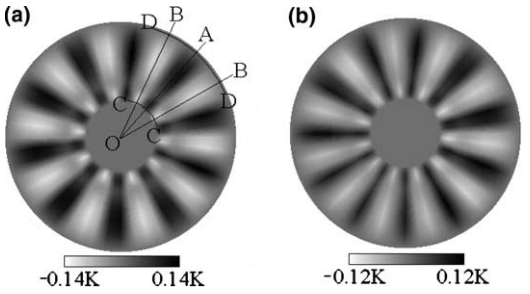

Fig. 4. Snapshots of surface temperature fluctuation at $\Delta T = 16$ K ($Ma = 16.3$) for the steady 3-D flow: (a) case A; (b) case B.

(see Fig. 7(b)), and the second critical Marangoni number Ma_{cri2} are tabulated in Table 2.

Fig. 8 shows simulation results above the second critical point for case A, including the distribution of surface temperature fluctuation δT and an STD of surface temperature along a circumference at $r = 20$ mm. In case A, when the temperature difference slightly exceeds the second critical value, for example $\Delta T = 18$ K ($Ma = 18.3$), the rotation is not complete and the spokes exhibit irregular oscillations back and forth in the azimuthal direction, as shown in Fig. 8(a). In this case, the STD shows a set of wavy lines. Under larger temperature difference, $\Delta T = 21$ K ($Ma = 21.3$) as shown in Fig. 8(b), many traveling curved spokes are observed on the melt surface. Fig. 8(d) shows the temperature oscillations at the monitoring point P. In this case, the curved spokes move along the counter-clockwise direction. With the increasing of the radial temperature difference, the angular velocity decreases slightly, but the amplitude of the temperature oscillations at the monitoring point P increases. These may correspond to the "hydrothermal wave". The angle (ϕ) between the wave propagation and the radial direction is approximately 78° at $r = 20$ mm, which is close to the angle of 80° predicted by the linear stability theory for infinite rectangular layer for $Pr = 0.01$ [1]. After ΔT exceeds about 25 K, the moving direction of the curved spokes changes abruptly from along the counter-clockwise to along the clockwise direction. Fig. 8(c) shows the results at $\Delta T = 27$ K $Ma = 21.4$). In this region, the angular velocity of the waves and the amplitude of the temperature oscillations at the monitoring point P increase with the increasing of the radial temperature difference, as shown in Fig. 6. For the molten silicon pool with $d = 3$ mm, the dynamic Bond number is $Bo = Ra/Ma = 0.48$. That means that Ma number is around twice Ra number. Therefore, thermocapillary forces are dominant and

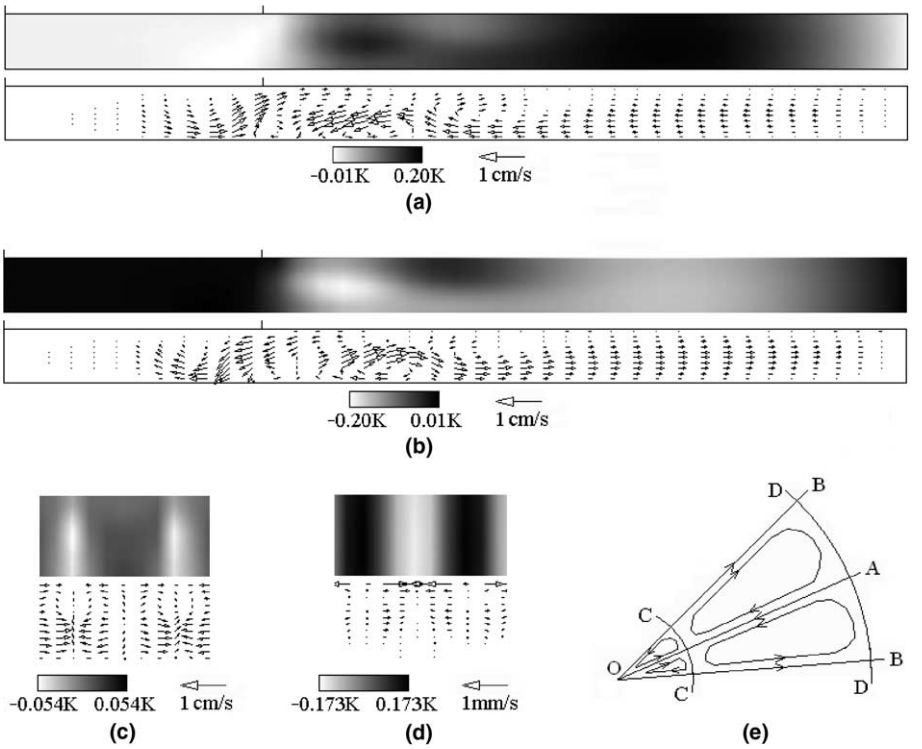

Fig. 5. Temperature fluctuation and fluctuation velocity vectors at different sections marked in Fig. 4(a): section O–A; (b) section O–B; (c) section C–C ($r = 15.6$ mm); (d) section D–D ($r = 47.2$ mm) and (e) secondary circulating flow.

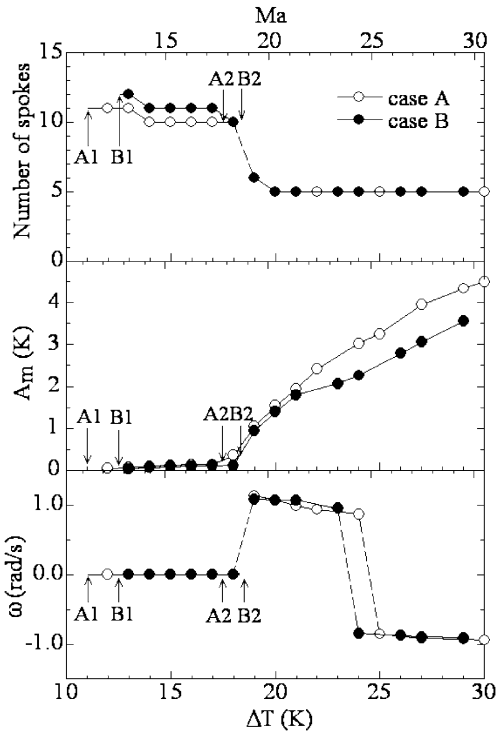

Fig. 6. Variation of number of spokes, amplitude of temperature oscillations at monitoring point P and angular velocity of wave propagation as functions of ΔT (Ma).

the hydrothermal wave instability is responsible for the oscillatory 3-D flow.

It should be noted that a similar two-step flow transition to an oscillatory flow is well known in the Marangoni convection in half-zone liquid bridge of low-Pr fluids [10–12]. In a half-zone liquid bridge, the first and second flow transitions are caused by hydrodynamic instability and the surface fluid flows against the thermocapillary force in the azimuthal direction. In the present case, however, on wide area of the melt surface, the surface fluid flows in the same direction as that of thermocapillary force.

For case B, the flow patterns are almost the same as those of the case A, as shown in Fig. 9. This fact suggests that the small vertical heat flux does not cause significant effects on the 3-D flow patterns in the silicon melt in a shallow pool with the Cz configuration. The number of the curved spokes and the angular velocity of the wave propagation are independent of the thermal boundary conditions at the bottom and free surface. However, the amplitude of the temperature oscillations at the point P is slightly less than that of case A, as shown in Fig. 6. Fig. 9(c) shows the experimental result reported by Azami et al. [6]. The surface patterns look similar to those of the numerical simulation. However, it is found that the traveling speeds in the azimuthal direction in the present simulation are slower than those of experiments. Difference in the geometric size, uncertainties in the thermal boundary conditions in the experiments and also uncertainty of the temperature coefficient of surface tension of silicon melt may be attributed to the cause of the discrepancy.

4. Conclusions

A series of 3-D numerical simulations of thermocapillary-buoyancy flow in shallow silicon melt pools with the Cz configuration were conducted by means of the finite difference method. The numerical results reveal that the Cz configuration changes the stability and the characteristics of the induced 3-D flow patterns from those in an annular pool.

A two-step flow transition process leads the steady 2-D flow to a 3-D oscillatory flow. At the first critical condition, a 2-D steady flow changes to a stationary 3-D flow with straight spokes on the melt surface and at the second critical condition flow exhibits a transition from the steady 3-D flow to an oscillatory 3-D flow with many curved spokes traveling in the azimuthal direction, i.e., hydrothermal waves.

The critical temperature differences for the flow transitions were determined for adiabatic pools and pools

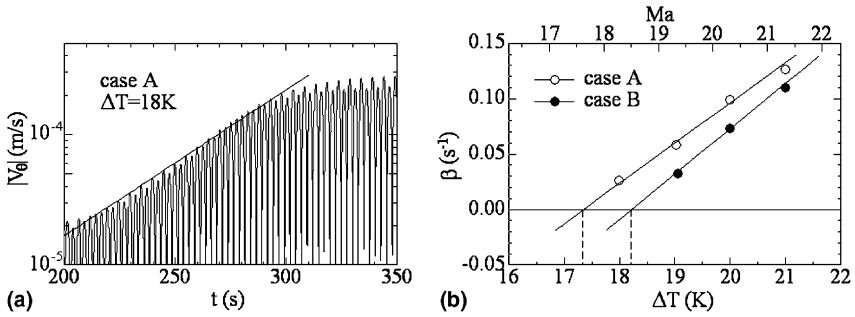

Fig. 7. Determination of the second critical point: (a) growth of the azimuthal velocity disturbances at monitoring point P; (b) β vs. $\Delta T(Ma)$ plot for determining $\Delta T_{cri2}(Ma_{cri2})$.

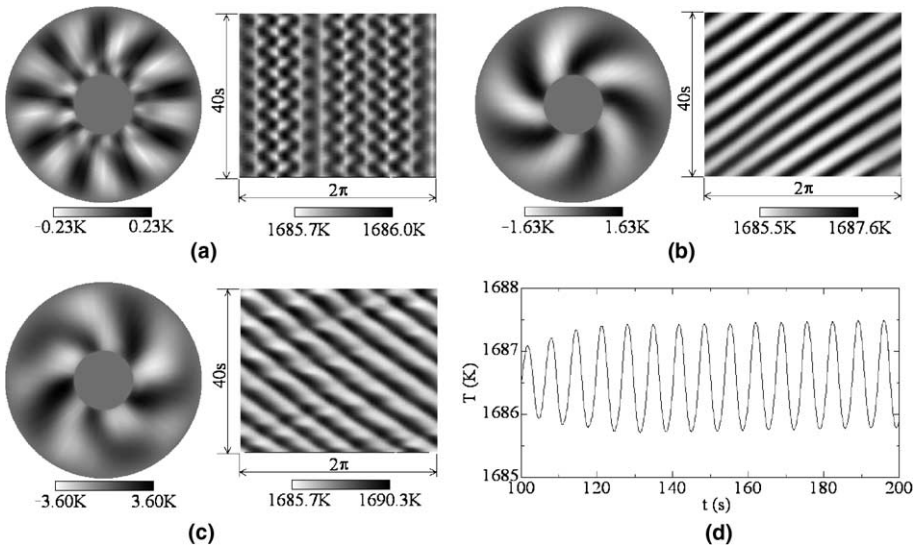

Fig. 8. Snapshots of surface temperature fluctuation and STD of surface temperature distribution of the oscillatory 3-D flow at $r = 20$ mm for case A: (a) $\Delta T = 18$ K ($Ma = 18.3$); (b) $\Delta T = 21$ K ($Ma = 21.3$); (c) $\Delta T = 27$ K ($Ma = 27.4$) and (d) temperature oscillations at the monitoring point P for case A at $\Delta T = 21$ K ($Ma = 21.3$).

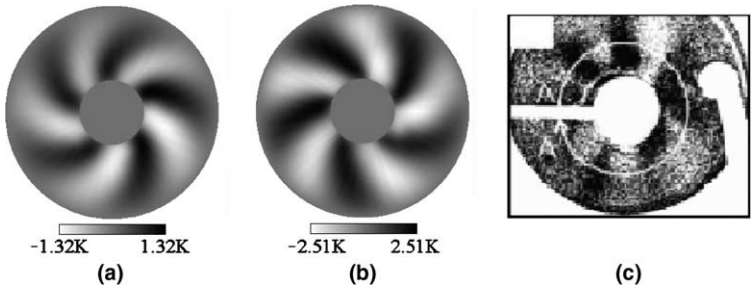

Fig. 9. Snapshots of surface temperature fluctuation for case B: (a) $\Delta T = 21$ K ($Ma = 21.3$); (b) $\Delta T = 27$ K ($Ma = 27.4$) and (c) experimental result [6].

accompanying a small vertical heat flux. The critical values for the incipience of hydrothermal wave are significantly larger than those in annular pools with inner cylindrical cold wall determined in our previous work [7].

Acknowledgement

Y. R. Li acknowledges the kind invitation of Prof. N. Imaishi, the Director of Institute for Materials Chemistry and Engineering of Kyushu University, for him to be a visiting Professor in Kyushu University. This simulation is done mostly during his visiting period, and was completed when he returned to Chongqing University. This work is supported by National Natural Science Foundation of China (grant number 50476042).

References

[1] M.K. Smith, S.H. Davis, Instabilities of dynamic thermocapillary liquid layers. Part 1. Convective instabilities, J. Fluid Mech. 132 (1983) 119–144.
[2] P. Laure, B. Roux, Linear and non-linear analysis of the Hadley circulation, J. Cryst. Growth 97 (1989) 226–234.
[3] H. Yamagishi, I. Fusegawa, Experimental observation of a surface pattern on a Caochralski silicon melt, J. Jpn. Assoc. Cryst. Growth 17 (1990) 304–311.
[4] K.W. Yi, K. Kakimoto, M. Eguchi, M. Watanabe, T. Shyo, T. Hibiya, Spoke patterns on molten silicon in Czochralski system, J. Cryst. Growth 144 (1994) 20–28.
[5] S. Nakamura, M. Eguchi, T. Azami, T. Hibiya, Thermal waves of a nonaxisymmetric flow in a Czochralski-type silicon melt, J. Cryst. Growth 207 (1999) 55–61.
[6] T. Azami, S. Nakamura, M. Eguchi, T. Hibiya, The role of surface-tension-driven flow in the formation of a surface

pattern on a Czochralski silicon melt, J. Cryst. Growth 233 (2001) 99–107.
[7] Y.R. Li, N. Imaishi, T. Azami, T. Hibiya, Three-dimensional oscillatory flow in a thin annular pool of silicon melt, J. Cryst. Growth 260 (2004) 28–42.
[8] S.V. Patankar, Numerical Heat Transfer and Fluid Flow, Hemisphere Publishing Co., 1980.
[9] Y.R. Li, L. Peng, Y. Akiyama, N. Imaishi, Three-dimensional numerical simulation of thermocapillary flow of moderate Prandtl number fluid in an annular pool, J. Cryst. Growth 259 (2003) 374–387.
[10] M. Wanschura, V.M. Shevtsova, H.C. Kuhlmann, H.J. Rath, Convective instability mechanisms in thermocapillary liquid bridges, Phys. Fluids 5 (1995) 912–925.
[11] M. Levenstam, G. Amberg, Hydrodynamical instabilities of thermocapillary flow in a half-zone, J. Fluid Mech. 297 (1995) 357–382.
[12] N. Imaishi, S. Yasuhiro, Y. Akiyama, S Yoda, Numerical simulation of oscillatory Marangoni flow in half-zone liquid bridge of low Prandtl number fluid, J. Cryst. Growth 230 (2001) 164–171.